Improvements to a novel learning algorithm for model-based wind turbine controllers

Fechner, U.; Spagnolo, F.; Mulders, S. P.

DOI
10.1088/1742-6596/2767/3/032013

Publication date
2024

Document Version
Final published version

Published in
Journal of Physics: Conference Series

Improvements to a novel learning algorithm for model-based wind turbine controllers

Journal of Physics: Conference Series **2767** (2024) 032013 doi:10.1088/1742-6596/2767/3/032013

Improvements to a novel learning algorithm for model-based wind turbine controllers

U Fechner[1], F Spagnolo[2], SP Mulders[1]

[1]Delft University of Technology, DCSC, Mekelweg 2, 2628 CD Delft, The Netherlands
[2]Vestas Wind Systems A/S, Hedeager 42, 8200 Aarhus N, Denmark

E-mail: u.fechner-1@tudelft.nl

Abstract. Wind turbine controllers are nowadays ever more advanced and rely on accurate internal controller model information. Therefore a calibrated model is needed for attaining predictable controller performance and ensuring stable operation. To calibrate the internal model information, a novel learning control scheme has recently been proposed that exploits the dynamics of the closed-loop controlled wind turbine system, without the need for wind speed measurements. The learning algorithm thereby periodically excites the generator power controller input signal. An extremum-seeking demodulation scheme was used to calibrate the internal model information. This paper improves the existing learning scheme in two ways: Firstly, it investigates how the frequency of the excitation signal influences the signal-to-noise ratio. Secondly, the problem was reformulated as a root-finding problem. This requires using the in-phase component of the phase-corrected learning signal. In addition, a precalculated lookup table relates the measured in-phase component directly to model uncertainty. It was found that an increased excitation frequency improves the signal-to-noise ratio (SNR) by an order of magnitude. Combined, these contributions improve the convergence speed more than twenty times, addressing the effect of aerodynamic degradation and its consequences on controller performance.

1. Introduction

The Intergovernmental Panel on Climate Change report from 2023 concludes that "There is a rapidly closing window of opportunity to secure a liveable and sustainable future for all", noting that very steep reductions of greenhouse gas emissions are now necessary to limit warming to 1.5C [1]. A 43% reduction in emissions by 2030 is now needed to reach this target [1], thus requiring a very fast transition to renewable energies, and new wind energy on land was in 2022 the cheapest form of renewable energies [2]. To reach this goal it is not only required to deploy new turbines but also to extend the lifetime of existing turbines.

An accurate internal controller model is required for the efficient and reliable operation of aging wind turbines [3]. Past research investigated the average performance degradation for a large ensemble of turbines [4], but this method is not directly applicable to single turbines. In [5] a sophisticated method for estimating both the power coefficient and the rotor effective wind speed of a wind turbine was presented. It is based on Gaussian regression and Kalman filtering but has the limitation that accurate measurements of the wind speed at hub height need to be available.

This is not required for the novel learning control scheme [6] that has recently been proposed, which exploits the dynamics of the closed-loop controlled wind turbine system. Therefore with

this research, we focus on ways to estimate the performance degradation of a single wind turbine that could be used to recalibrate the internal model. The algorithm excites the controller input signal and a real-time demodulation scheme is used to calibrate the internal model information. It makes use of the convex property of the magnitude response between the generator control input and the power estimation error to diminish under increasing model accuracy. However, the scheme as presented in [6] shows slow convergence and is not reliable in high wind turbulence. More specifically, this is caused by high noise levels due to wind turbulence.

This paper improves the existing learning scheme on the previously mentioned issues, and thereby proposes two contributions: Firstly, this paper investigates how the frequency of the excitation signal influences the signal-to-noise ratio. Secondly, the problem was reformulated as a root-finding problem, which allows much faster convergence in the presence of noise than solving a convex optimization problem. The new approach requires using the in-phase component of the phase-corrected learning signal instead of the amplitude. The in-phase component is signed, and the sign indicates whether the estimate is too high or too low which allows fast convergence. In addition, a pre-calculated lookup table relates the measured in-phase component directly to model uncertainty. It also allows the calculation of an updated standard deviation of the model uncertainty after each measurement.

The paper is structured as follows: First, in the Section 2, the turbine model and controller, assumptions and uncertainty modeling are explained. Then, Section 3 entails the first contribution, by presenting a derivation of an analytical and frequency-dependent signal-to-noise expression. Then follows the second contribution, the improved learning algorithm in Section 4. Finally, we present the simulation results in Section 5, draw conclusions and provide an outlook in Section 6.

2. Turbine model and controller, assumptions and uncertainty modeling

In this section, we provide the required background information about the system to which the learning control will be applied. First, the dynamic system model is explained, then the uncertainty modeling framework is introduced.

2.1. Turbine model, controller and wind speed estimator

This section defines the fundamental relations that constitute the full dynamic system with partial load control as depicted in Fig. 1. To this end, first, the wind turbine is defined, which

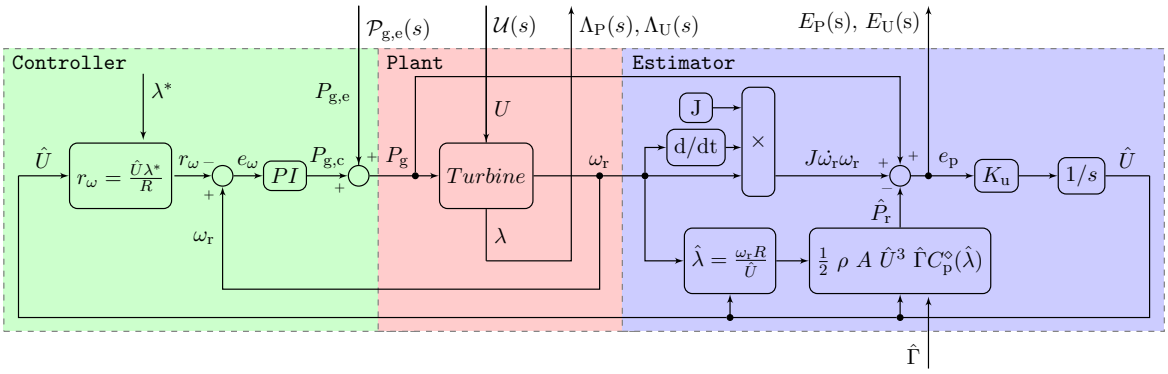

Figure 1. Block diagram of the turbine controller, turbine and wind speed estimator [6]. The system has the inputs U (REWS), $P_{g,e}$ (excitation power) and $\hat{\Gamma}$ and the outputs λ (tip speed ratio) and e_p (measured error signal). When the modeled $\hat{\Gamma} C_p^\diamond$ matches the actual turbine aerodynamic properties C_p the error signal becomes zero in steady-state conditions.

is modeled as a first-order system

$$J\dot{\omega}_{\mathrm{r}}\omega_{\mathrm{r}} = P_{\mathrm{r}} - P_{\mathrm{g}} \ , \tag{1}$$

in which J is the effective rotor inertia at the low-speed shaft, ω_{r} the rotor speed, P_{r} the aerodynamic rotor power and P_{g} the mechanical generator power. It is assumed that this generator power can be controlled directly.

The aerodynamic power is given by

$$P_{\mathrm{r}} = \frac{1}{2}\ \rho A U^3\ C_{\mathrm{P}}(\lambda) \ , \tag{2}$$

where ρ is the air density, A the rotor area, U the rotor effective wind speed (REWS) and $C_{\mathrm{P}}(\lambda)$ the power coefficient as a function of the tip speed ratio $\lambda = \omega_{\mathrm{r}}R/U$, with R being the rotor radius. The REWS, defined as the average wind speed on the rotor surface [7] is estimated using the following dynamic power balance equation:

$$\dot{\hat{U}} = K_{\mathrm{U}}\ e_{\mathrm{P}} = K_{\mathrm{U}}\ \left(P_{\mathrm{g}} - \hat{P}_{\mathrm{r}} + J\dot{\omega}_{\mathrm{r}}\omega_{\mathrm{r}}\right), \tag{3}$$

where K_{U} is the estimator gain, and the estimated aerodynamic rotor power is defined as

$$\hat{P}_{\mathrm{r}} = \frac{1}{2}\ \rho A\hat{U}^3\ \hat{C}_{\mathrm{P}}(\hat{\lambda}), \tag{4}$$

with $\hat{\lambda} = \omega_{\mathrm{r}}R/\hat{U}$, and $\hat{C}_{\mathrm{P}}$ is the estimated model for the power coefficient and will be defined in the second part of this section.

The controller for the tip-speed-ratio (TSR) is a proportional-integral (PI) controller that uses the estimated rotor effective wind speed $\hat{U}$ and the set point of the tip speed ratio λ^* to calculate the set point of the rotor speed:

$$r_\omega = \frac{\hat{U}\lambda^*}{R}\ . \tag{5}$$

The PI controller is defined by

$$\dot{P}_{\mathrm{g}} = K_{\mathrm{P}}\dot{e}_\omega + K_{\mathrm{i}}e_\omega \ , \tag{6}$$

in which the error $e_\omega = -(r_\omega - \omega_{\mathrm{r}})$ is the negative difference between the setpoint and the actual rotor speed ω_{r}. We use the negative difference here for K_{P} and K_{i} to be positive.

2.2. Assumptions and uncertainty modeling

As shown in the purple estimator block in Fig. 1, the REWS estimator employs aerodynamic model information of the actual turbine. Inconsistent model information results in a biased value of the estimated REWS $\hat{U}$. As this estimate is used as a feedback signal, this results in sub-optimal power extraction [3] and in the worst case a loss of stability. For the considered learning algorithm, uncertainty is only considered for the power coefficient information using the uncertainty framework introduced next. The algorithm proposed in [6] used scalar multiplicative uncertainty in the power coefficient: We make the same assumption. Multiplicative uncertainty on the ideal power coefficient information for the actual turbine is indicated by the degradation factor $\Gamma \in \mathbb{R}^+$ for the actual turbine, and by $\hat{\Gamma} \in \mathbb{R}^+$ for the estimator model:

$$C_{\mathrm{P}}(\lambda) = \Gamma\ C_{\mathrm{p}}^{\diamond}(\lambda)\ , \quad \hat{C}_{\mathrm{P}}(\hat{\lambda}) = \hat{\Gamma}\ C_{\mathrm{p}}^{\diamond}(\hat{\lambda})\ , \tag{7}$$

where $C_{\mathrm{p}}^{\diamond}$ is the original function for the power coefficient as function of the tip speed ratio, representing nominal (non-degraded) power coefficient characteristics [6]. Fig. 2 illustrates the concept of multiplicative uncertainty for different values of Γ. The goal is to estimate Γ and calibrate $\hat{\Gamma}$ accordingly in this learning scheme.

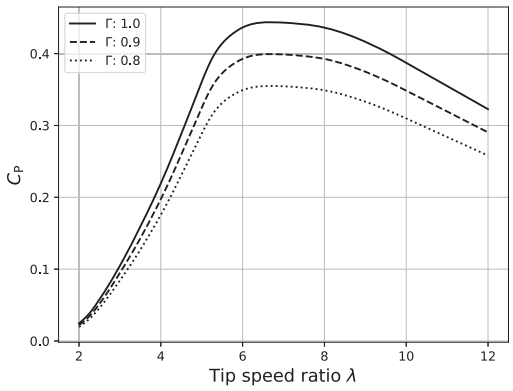

Figure 2. Power coefficient C_P as function of the tip speed ratio λ of the NREL 5MW reference turbine. Plotted is the original $C_\mathrm{P}^\diamond$ function, and the C_P curves for a degradation factor of $\Gamma = 0.9$ and $\Gamma = 0.8$.

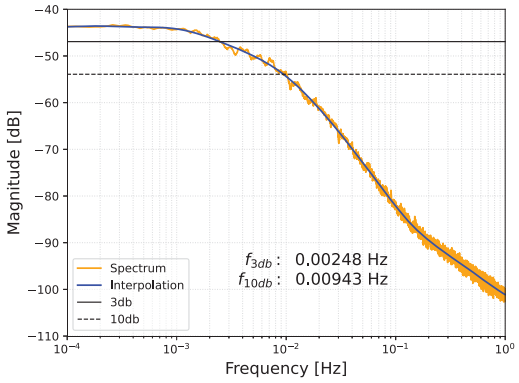

Figure 3. Spectrum of the rotor effective wind speed (REWS) at a wind speed of 7 m/s and a turbulence intensity at hub height of 4.5%, which results in 3% turbulence intensity of the REWS.

3. Derivation of the signal-to-noise ratio

The learning algorithm as proposed in [5] works in the following way: In the wind speed estimator, a power balance is calculated by substracting the estimated rotor power from the generator power and adding the power needed to accelerate the rotor. If the performance factor $\hat{\Gamma}$ is too large or too small, the excitation signal $P_\mathrm{g,e}$ will appear in e_p with a sign that indicates if $\hat{\Gamma}$ is too large or too small. To improve the detectability of the excitation in the error signal with the aim to improve the convergence of the algorithm [6], we need to understand on which parameters the signal-to-noise ratio of the excitation power in the error signal with respect to the power of the wind disturbance is depending.

The learning scheme excites the system input with a generator power excitation signal $P_\mathrm{g,e}$ and the error signal e_p on the right-hand side is measured, as shown in Fig. 1. Therefore we define a frequency-dependent expression for the signal-to-noise-ratio (SNR):

$$\mathrm{SNR}(s) = \frac{E_\mathrm{P}(s)}{E_\mathrm{U}(s)} , \tag{8}$$

where s is the Laplace operator. The expression is the ratio of the power of the detected excitation signal $E_\mathrm{P}(s)$ and the power of the REWS turbulence $E_\mathrm{U}(s)$. The next section provides an analytical derivation for this expression to identify the parameters that affect it.

3.1. Transfer functions of the closed loop dynamic system

To explain the derivation of the SNR it is necessary to consider the block diagram of the closed-loop dynamic system in Fig. 1. First, the following transfer functions (TFs) are defined:

$$\mathcal{H}(s) = E_\mathrm{P}(s)/\mathcal{P}_\mathrm{g,e}(s) , \quad \mathcal{J}(s) = E_\mathrm{U}(s)/\mathcal{U}(s). \tag{9}$$

Now by substitution of Eq. (9) in Eq. (8) we obtain

$$\mathrm{SNR}(s) = \frac{E_p(s)}{E_U(s)} = \frac{\mathcal{H}(s)\mathcal{P}_\mathrm{g,e}(s)}{\mathcal{J}(s)\mathcal{U}(s)} . \tag{10}$$

A third transfer function is introduced and used to substitute $\mathcal{P}_{\mathrm{g,e}}$ to get the TSR amplitude-dependent expression:

$$\mathcal{I}(s) = \Lambda_{\mathrm{P}}(s)/\mathcal{P}_{\mathrm{g,e}}(s) \ , \tag{11}$$

and to arrive at

$$\mathrm{SNR}(s) = \underbrace{\frac{\mathcal{H}(s)}{\mathcal{J}(s)\mathcal{I}(s)}}_{\text{TFs}} \ \underbrace{\frac{1}{\mathcal{U}(s)}}_{\text{Wind spectrum}} \ \underbrace{\Lambda_{\mathrm{P}}(s)}_{\text{TSR amplitude}} \ . \tag{12}$$

Now, under the condition that the TSR constraint is constant over all frequencies, we can say that $\Lambda_{\mathrm{P}}(s) = A_\lambda$, so that we get the result

$$\mathrm{SNR}(s) = \frac{\mathcal{H}(s)}{\mathcal{J}(s)\mathcal{I}(s)} \ \frac{A_\lambda}{\mathcal{U}(s)} \ . \tag{13}$$

This equation relates the SNR to the excitation frequency using three transfer functions of the system, the TSR amplitude and the wind speed spectrum: Higher amplitudes of the tip speed ratio λ increase the SNR, and a higher amplitude of the wind turbulence $\mathcal{U}(s)$ decreases it. The first fraction consisting of closed-loop system TFs will be derived in the next section.

3.2. Analytic derivation of the closed-loop transfer functions
We define the left term of the right-hand side of Eq. (13) as

$$\mathcal{L}(s) = \frac{\mathcal{H}(s)}{\mathcal{J}(s)\mathcal{I}(s)} \tag{14}$$

and investigate it analytically. Before providing the linear derivation, the (estimated) power coefficient functions are assumed as a linear affine approximation at the considered operating points:

$$C_{\mathrm{P}}^{\diamond}(\lambda) = a\lambda + b \ , \quad C_{\mathrm{P}}^{\diamond}(\hat{\lambda}) = c\hat{\lambda} + d \ . \tag{15}$$

We need to derive the functions $\mathcal{H}(s)$, $\mathcal{J}(s)$ and $\mathcal{I}(s)$ and combine and simplify them to derive $\mathcal{L}(s)$. The following section starts with a time-domain (state-space system) derivation and is later converted to the frequency domain to arrive at an analytic expression for $\mathcal{J}(s)$. As the derivation of the other two transfer functions follows a similar procedure, only the result is given at the end of this section.

3.2.1. Derivation of $\mathcal{J}(s)$ As the first step, we derive the state space system of the nonlinear plant, which consists of the wind turbine in series with the wind speed estimator as defined in Section 2.1. The state, input and output vectors are respectively defined as

$$\mathbf{x} = \begin{bmatrix} \omega_{\mathrm{r}} \\ \hat{U} \end{bmatrix} \ , \quad \mathbf{u} = \begin{bmatrix} U \\ P_{\mathrm{g,c}} \end{bmatrix} \ , \quad \mathbf{y} = \begin{bmatrix} e_\omega \\ e_{\mathrm{P}} \end{bmatrix} . \tag{16}$$

We use the linear power coefficient function approximations of Eq. (15). When linearizing the state space system of the plant, assuming $P_{\mathrm{g,e}} = 0$ we obtain

$$\mathbf{A}_{\mathrm{p}} = \begin{bmatrix} \frac{\bar{P}_{\mathrm{g}} - 0.5Ab\Gamma\rho U^3}{J\bar{\omega}_{\mathrm{r}}^2} & 0 \\ K_u\left(0.5U^2 ARa\Gamma\rho - 0.5\hat{U}^2 ARc\hat{\Gamma}\rho\right) & -K_u V \end{bmatrix}, \tag{17}$$

$$\mathbf{B}_{\mathrm{p}} = \begin{bmatrix} \frac{1.5U^2 Ab\Gamma\rho + ARUa\Gamma\rho\bar{\omega}_{\mathrm{r}}}{J\bar{\omega}_{\mathrm{r}}} & \frac{-1}{J\bar{\omega}_{\mathrm{r}}} \\ \left(-0.5ARUa\Gamma\rho\bar{\omega}_{\mathrm{r}} + 1.5A\left(b\ U + Ra\bar{\omega}_{\mathrm{r}}\right)U\Gamma\rho\right)K_{\mathrm{u}} & 0 \end{bmatrix}, \tag{18}$$

$$\mathbf{C}_{\mathrm{p}} = \begin{bmatrix} -1 & \frac{\lambda^*}{R} \\ Q - \hat{Q} & -V \end{bmatrix} \ , \quad \mathbf{D}_{\mathrm{p}} = \mathbf{0} \tag{19}$$

where $\bar{P}_\mathrm{g}$ is the equilibrium point of the generator power used for the linearization, and $\bar{\omega}_\mathrm{r}$ the equilibrium point of the rotor speed. The following terms are introduced to simplify the results:

$$\begin{aligned} &Q = 0.5U^2 ARa\Gamma\rho \ , \quad \hat{Q} = 0.5\hat{U}^2 ARc\hat{\Gamma}\rho \ , \\ &V = 1.5A\hat{\Gamma}\rho\hat{U}(d\hat{U} + Rc\bar{\omega}_\mathrm{r}) + 0.5ARc\hat{\Gamma}\rho\hat{U}\bar{\omega}_\mathrm{r} \ . \end{aligned} \tag{20}$$

Now the PI controller is constructed in state-space notation:

$$\mathbf{A}_\mathrm{c} = 0 \ , \quad \mathbf{B}_\mathrm{c} = 1 \ , \quad \mathbf{C}_\mathrm{c} = K_\mathrm{i} \ , \quad \mathbf{D}_\mathrm{c} = K_\mathrm{p} \tag{21}$$

Connecting the plant and the controller results in the following, combined state space model with the input and output

$$\mathbf{u} = U \ , \quad \mathbf{y} = e_\mathrm{P} \tag{22}$$

and the matrices

$$\mathbf{A} = \begin{bmatrix} \frac{\bar{P}_\mathrm{g} + K_\mathrm{p}\bar{\omega}_\mathrm{r} - 0.5U^3 Ab\Gamma\rho}{\bar{\omega}_\mathrm{r}^2 J} & \frac{-K_\mathrm{p}\lambda^*}{JR\bar{\omega}_\mathrm{r}} & \frac{-K_\mathrm{i}}{J\bar{\omega}_\mathrm{r}} \\ \left(Q - \hat{Q}\right) K_\mathrm{u} & -K_\mathrm{u} V & 0 \\ -1 & \frac{\lambda^*}{R} & 0 \end{bmatrix} \tag{23}$$

$$\mathbf{B} = \begin{bmatrix} \frac{1.5U^2 Ab\Gamma\rho + ARUa\bar{\omega}_\mathrm{r}\Gamma\rho}{J\bar{\omega}_\mathrm{r}} \\ \left(-0.5ARUa\bar{\omega}_\mathrm{r}\Gamma\rho + 1.5A\left(b\ U + Ra\bar{\omega}_\mathrm{r}\right) U\Gamma\rho\right) K_\mathrm{u} \\ 0 \end{bmatrix} \tag{24}$$

$$\mathbf{C} = \begin{bmatrix} \left(Q - \hat{Q}\right) & -V & 0 \end{bmatrix} \tag{25}$$

$$\mathbf{D} = \ 1.5U^2 A\left(b + \tfrac{Ra\bar{\omega}_\mathrm{r}}{U}\right)\Gamma\rho - 0.5ARUa\Gamma\rho\bar{\omega}_\mathrm{r} \tag{26}$$

A unique transfer function representation of the combined state-space system in Eq. (23) to (26) is obtained using $\mathbf{C}\ (s\mathbf{I} - \mathbf{A})^{-1}\ \mathbf{B} + \mathbf{D}$, resulting in

$$\mathcal{J}(s) = \frac{b_3 s^3 + b_2 s^2 + b_1 s}{a_3 s^3 + a_2 s^2 + a_1 s + a_0}, \tag{27}$$

representing the transfer function from the wind input to the wind speed estimation error, with the coefficients defined as:

$$\begin{aligned} b_3 &= -ARU\Gamma\rho\left(3b\ U + 2Ra\bar{\omega}_\mathrm{r}\right)\bar{\omega}_\mathrm{r}^2 J \\ b_2 &= ARU\Gamma\rho\left(3b\ U + 2Ra\bar{\omega}_\mathrm{r}\right)\left(P_\mathrm{g} + \left(\hat{Q} - Q + K_\mathrm{p} + K_\mathrm{i}\right)\bar{\omega}_\mathrm{r} - 0.5U^3 Ab\Gamma\rho\right) \\ b_1 &= ARU\Gamma\rho\ K_\mathrm{i}\bar{\omega}_\mathrm{r}\left(3b\ U + 2Ra\bar{\omega}_\mathrm{r}\right) \end{aligned} \tag{28}$$

$$\begin{aligned} a_3 &= -4\ \bar{\omega}_\mathrm{r}^2 JR \\ a_2 &= 2\ \left(2\bar{P}_\mathrm{g} R + 2K_\mathrm{p} R\bar{\omega}_\mathrm{r} - 2\bar{\omega}_\mathrm{r}^2 JK_\mathrm{u} RV - U^3 ARb\Gamma\rho\right) \\ a_1 &= 4\ \left(K_\mathrm{i} R\bar{\omega}_\mathrm{r} + K_\mathrm{u}\bar{P}_\mathrm{g} RV - K_\mathrm{p} K_\mathrm{u} Q\lambda^*\bar{\omega}_\mathrm{r} + K_\mathrm{p} K_\mathrm{u}\hat{Q}\lambda^*\bar{\omega}_\mathrm{r} + K_\mathrm{p} K_\mathrm{u} RV\bar{\omega}_\mathrm{r} - 0.5U^3 AK_\mathrm{u} RVb\Gamma\rho\right) \\ a_0 &= 4K_\mathrm{i} K_\mathrm{u}((\hat{Q} - Q)\lambda^*\bar{\omega}_\mathrm{r} + RV\bar{\omega}_\mathrm{r}) \end{aligned} \tag{29}$$

The transfer functions $\mathcal{H}(s)$ and $\mathcal{I}(s)$ are obtained using a similar procedure. For brevity, these transfer functions are not derived here. The individual results are validated using the numerical linearization capabilities of the Julia package ModelingToolkit.jl [8] on a symbolic definition of the full nonlinear system.

3.2.2. Simplification of $\mathcal{L}(s)$ with the definition of $\mathcal{J}(s)$, $\mathcal{H}(s)$ and $\mathcal{I}(s)$ at hand, $\mathcal{L}(s)$ can be calculated using Eq. (14), and it can be split into a constant, frequency-independent term K and the frequency-dependent s term $\mathcal{L}_r(s)$

$$\mathcal{L}(s) = K\ \mathcal{L}_r(s) = \frac{U^2 a\Gamma - \hat{U}^2 c\ \hat{\Gamma}}{(3Ub + 2Ra\omega_\mathrm{r})\ \Gamma}\ \frac{s^3 + b_2 s^2 + b_1 s + b_0}{s^3 + a_2 s^2 + a_1 s + a_0}\ . \tag{30}$$

We define the relative differences:

$$d_2 = \frac{b_2 - a_2}{b_2}\ , \quad d_1 = \frac{b_1 - a_1}{b_1}\ , \quad d_0 = \frac{b_0 - a_0}{b_0}\ . \tag{31}$$

If $|d_2|$, $|d_1|$ and $|d_1|$ are all $\ll 1$ we can assume $\mathcal{L}_r(s) \approx 1$. In $\mathcal{L}_r(s)$ the coefficients of the highest power of s in the numerator and denominator are the same. The other coefficients only differ by a term proportional to $\Gamma - \hat{\Gamma}$. Therefore, for $(\Gamma - \hat{\Gamma}) \to 0$ numerator and denominator of $\mathcal{L}_r$ cancel out and the term approaches the value of one.

Under the resulting assumption that $\Gamma/\hat{\Gamma}$ is close to one, the following approximate analytical frequency-dependent SNR expression is obtained:

$$\mathrm{SNR}(s) \approx \frac{U^2 a\Gamma - \hat{U}^2 c\ \hat{\Gamma}}{(3Ub + 2Ra\omega_\mathrm{r})\ \Gamma}\ \frac{1}{\mathcal{U}(s)} A_\lambda\ . \tag{32}$$

The SNR depends dynamically on the inverse of the rotor effective wind speed spectrum: therefore a higher excitation frequency results in an improved signal-to-noise ratio. Furthermore, the SNR depends statically on the amplitude of imposed TSR variations, the turbine operating point and the degree of turbine degradation. It is concluded that higher TSR amplitudes result in an overall increased SNR (among all frequencies). Furthermore the coefficients a, b, c that depend on the shape and height of the function $C_\mathrm{P} = f(\lambda)$ influence the SNR. A difference between the gradients a and c of $C_\mathrm{P}^\diamond$ at the real and the estimated TSR improves the SNR.

Notably, the expression shows that the SNR is independent of the inertia of the turbine and of the controller parameters K_i, K_p and K_u under the assumption that the system is stable.

3.3. Numerical evaluation and further insights

Numerical simulations were performed to better understand the analytical SNR expression of Eq. (32). For that we need the spectra $\mathcal{U}(s)$ of the rotor effective wind speed. It was derived from a 3D wind field for an average wind speed of 7 m/s and turbulence intensity at hub height of 4.5%, and was generated using PyConTurb [9] using the Kaimal spectrum. The spectrum of this data set is shown in Fig. 3.

For the simulation the NREL 5-MW reference turbine [10] at 90 m hub height was used. The most important parameters can be found in Tab. 1. The investigation was done for a minimally degraded turbine with $\Gamma = 0.99$ and $\hat{\Gamma} = 1.0$. These values were chosen because the noise is mainly a problem when the estimated value is close to the real value. Fig 4 depicts the ratio of signal and noise, the function SNR(s). It can be seen that at low frequencies, signal and noise increase with the frequency with the same gradient, so the SNR(s) stays constant. At about 0.005 rad/s the increase in the noise level slows down to reach a maximum at about 0.05 rad/s, declining fast with a further increased frequency. In contrary, for frequencies above 0.3 rad/s, the signal stays constant. When combining signal and noise we therefore see a strong increase of the SNR for frequencies above 0.1 rad/s. An excitation frequency of 0.4382 rad/s was chosen, which results in an SNR of 20dB, but still stays well below the turbine structural resonances.

Table 1. Turbine, controller and estimator parameters

Variable	Value	Description	Unit
A	$1.247{\cdot}10^4$	Rotor area	m^2
R	63.0	Rotor radius	m
J	$4.047{\cdot}10^7$	Total inertia	$\mathrm{kg\,m}^2$
K_P	$4.426{\cdot}10^6$	Proportional gain	-
K_i	56824	Integral gain	-
K_U	$2.250{\cdot}10^{-7}$	Wind speed estimator gain	-
λ^*	8.0	Tip speed ratio set point	-
A_λ	0.5	TSR amplitude of the excitation	-

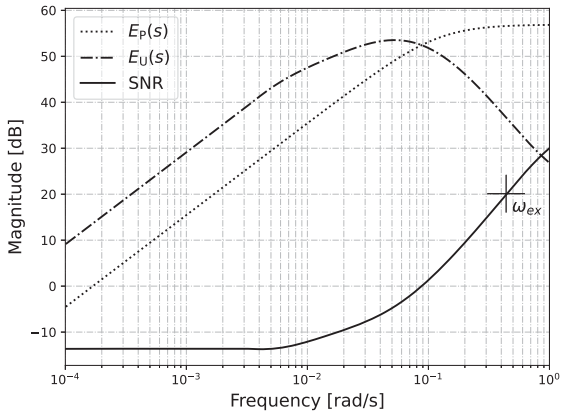

Figure 4. Signal-to-noise ratio of the excitation signal as measured at e_p as function of the excitation frequency. It can be seen that the SNR is proportional to the inverse $\mathcal{U}(s)$ as predicted by Eq. (32).

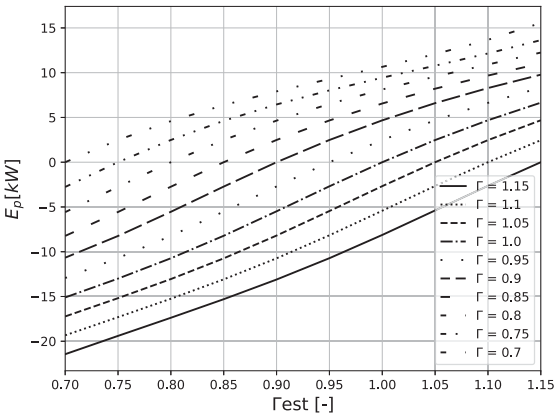

Figure 5. The in-phase signal amplitude as function of Γ and $\hat{\Gamma}$. This function is derived by simulation and interpolated using Chebychev polynomials.

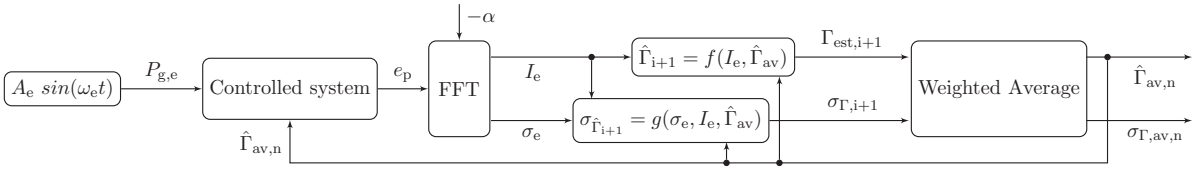

Figure 6. Block diagram of the advanced learning control scheme. It works iteratively. Every 30 min a new FFT is performed. The measured signal is phase-corrected by $-\alpha$ to compensate for the phase shift of the system.

4. The improved learning algorithm

After we explained how to choose a value for the excitation frequency that results in a high SNR and thus fast convergence, we explain the second contribution, the improved learning scheme.

4.1. Motivation

The learning scheme as proposed in [6] is based on real-time excitation-based gradient retrieval. The new method presented here collects data in batches for an extended period of time and uses root finding to calculate new estimates of the degradation factor Γ. In [6] an integrator was used to learn $\hat{\Gamma}$. Because of the high system nonlinearity for the considered input-output pair, finding the optimal integrator gain is challenging, and depending on the operating point will either produce an overshoot or converge very slowly. In addition, a real-time gradient-based optimization scheme has limited capabilities of including history, whereas the algorithm proposed here provides an ever-increasing accuracy the longer the measurement is ongoing.

4.2. Lookup tables

In the simulation, it is possible to measure the in-phase signal as a function of Γ and $\hat{\Gamma}$, which is a highly non-linear relationship as shown in Fig. 5. The results of these simulations can be used to create lookup tables, which can be approximated using a Chebychev function. This Chebychev function can easily be inverted to obtain $\Gamma = f(I_\mathrm{e}, \hat{\Gamma})$. When this function is known, under ideal conditions one measurement of I_e is sufficient to determine Γ. This function allows the learning algorithm to converge with optimal speed and little overshoot. A solution that is robust concerning model uncertainties can be obtained using an iterative scheme.

4.3. Implemented solution

A schematic representation of the iterative learning algorithm is shown in Fig. 6. It starts with an initial estimate of the degradation factor $\hat{\Gamma}_{\mathrm{av},0} = 1$. On the very left the excitation signal with the amplitude A_e excites the controlled system as shown in Fig. 1. The error signal e_p is collected for 30 mins. The FFT of the collected signal evaluated at ω_e is first turned by the constant phase shift α, which is the phase we loose at ω_e in the closed loop system. Then the real part represents the in-phase component I_e. The estimated standard deviation σ_e is calculated using the average amplitude of the 10 discrete frequencies above and below ω_e which represents the noise level present due to the wind turbulence.

The values of I_e as shown in Fig. 5 and the phase shift α are determined offline using the linearized system model. A Chebychev interpolation is used to interpolate I_e for any value of Γ and $\hat{\Gamma}$. The interpolated function is then inverted using a root-finding algorithm to obtain the function $\hat{\Gamma}_{\mathrm{i}+1} = f(I_\mathrm{e}, \hat{\Gamma}_\mathrm{av})$. The function $\sigma_{\hat{\Gamma}_{\mathrm{i}+1}} = g(\sigma_\mathrm{e}, I_\mathrm{e}, \hat{\Gamma}_\mathrm{av})$ is determined by differentiating the function $f(I_\mathrm{e}, \hat{\Gamma}_\mathrm{av})$.

The *Weighted Average* block uses the new estimates together with all older estimates to calculate every 30 min new, best estimates for the degradation and its standard deviation. The estimated degradation $\hat{\Gamma}_\mathrm{av}$ is fed back into the controlled system for the next measurement. It works as follows: The weight of each measurement should be proportional to the inverse square of the standard deviation [11]. This can be written as:

$$\hat{\Gamma}_{\mathrm{av,n}} = \frac{\sum_{i=1}^{n} x_i/\sigma_{\Gamma,i}^2}{\sum_{i=1}^{n} \sigma_{\Gamma,i}^2}\ , \quad \sigma_{\Gamma,\mathrm{av,n}} = \frac{1}{\sum_{\mathrm{i}=1}^{n} \sigma_{\Gamma,\mathrm{i}}^2}\ . \tag{33}$$

5. Simulation results of the learning scheme

In Fig. 7 the time domain results of a simulation of 11 hours are shown for an average wind speed at hub height of 7 m/s and a turbulence intensity of 4.5 %. The actual turbine degradation is $\Gamma = 0.85$, which is what shall be learned in this study. The three test cases differ concerning the seed of the random generator that created the wind time series. Thanks to the combined contributions of this work to the SNR and the improved iterative learning algorithm already after the first iteration (30 min) the $\hat{\Gamma}_\mathrm{av}$ is in the range of 0.825 to 0.875, and after 4h the 2σ confidence interval is down to ± 0.01 of the measured value.

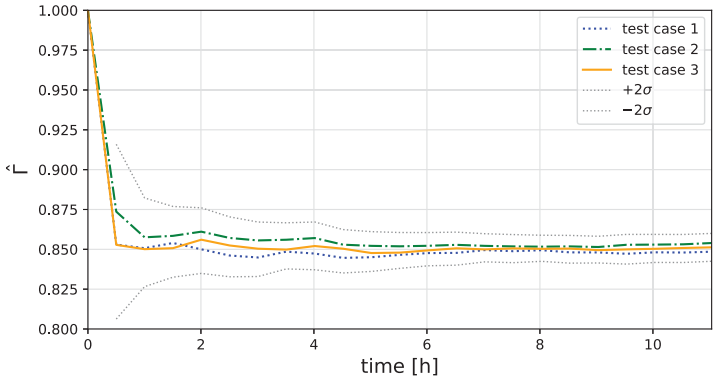

Figure 7. Progress of the learning of the degradation factor $\hat{\Gamma}$ for $\omega_e = 0.438$ rad/s and I=4.5%. Convergence is largely reached after the first iteration, with increasing certainty in subsequent iterations.

6. Conclusions and outlook

This paper proposed promising improvements to a wind speed measurement free learning scheme for model-based wind turbine controllers. Using the transfer functions of the model it was shown that a higher excitation frequency improves the signal-to-noise ratio and thus the convergence. A novel learning scheme further improves the convergence and provides a degradation estimate with ever-increasing accuracy. If these results can be verified in practice, then this new approach offers a promising way to auto-calibrate internal controller models of older wind turbines.

Furthermore, the foundations of the learning algorithm allow to detect and quantify possible damage to the turbine after a storm or similar weather events. Future research shall find out if not only a degradation of the power coefficient by a constant factor can be learned as explained in this paper, but also additional internal model parameters. Finally the algorithm was tested only for turbulence intensities up to 4.5% and it should be investigated if it is possible to adapt it for higher turbulence intensities.

References

[1] IPCC (2023): Climate Change 2023: Synthesis Report. Contribution of Working Groups I, II and III to the Sixth Assessment Report of the Intergovernmental Panel on Climate Change [Core Writing Team, H. Lee and J. Romero (eds.)]. IPCC, Geneva, Switzerland, pp. 35-115.

[2] IRENA (2023), Renewable power generation costs in 2022, International Renewable Energy Agency, Abu Dhabi ISBN 978-92-9260-544-5

[3] Brandetti, L. et al. (2022). On the ill-conditioning of the combined wind speed estimator and tip-speed ratio tracking control scheme. *TORQUE 2022: Journal of Physics – Conference Series.*

[4] Mathew, M. S., Kandukuri, S. T., & Omlin, C. W. (2022). Estimation of Wind Turbine Performance Degradation with Deep Neural Networks. PHM Society European Conference, 7(1), 351-359.

[5] Lio, W. H., Li, A., & Meng, F. (2021). Real-time rotor effective wind speed estimation using Gaussian process regression and Kalman filtering. Renewable Energy, 169, 670-686.

[6] Mulders, S., Brandetti, L., Spagnolo, F., Liu, Y., Christensen, P. & Wingerden, J (2023). A learning algorithm for the calibration of internal model uncertainties in advanced wind turbine controllers: A wind speed measurement-free approach. *2023 American Control Conference (ACC).*

[7] Jiao, X.; Yang, Q.; Zhu, C.; Fu, L.; Chen, Q (2019). Effective wind speed estimation and prediction based feedforward feedback pitch control for wind turbines. 2019 Asian Control Conference (ASCC).

[8] Yingbo Ma, Shashi Gowda, Ranjan Anantharaman, Chris Laughman, Viral Shah, and Chris Rackauckas. (2021). ModelingToolkit: A Composable Graph Transformation System For Equation-Based Modeling.

[9] Rinker, J (2018). PyConTurb: an open-source constrained turbulence generator. *TORQUE 2018: Journal Of Physics – Conference Series.*

[10] J. Jonkman, S. Butterfield, W. Musial, et al (2009). Definition of a 5-MW reference wind turbine for offshore system development, National Renewable Energy Laboratory (NREL), Tech. Rep.

[11] Statistics: A Guide to the Use of Statistical Methods in the Physical Sciences, Manchester Physics Series, Wiley Publishing, 1989